Sponge-like Heterogeneous Gels: Hierarchical Structures in Poly(*N*-isopropylacrylamide) Chemical Gels As Observed by Combined Scattering and Confocal Microscopy Method

Yoshitsugu Hirokawa,[†,‡] Takuya Okamoto,[†,§] Kohtaro Kimishima,[†,⊥] Hiroshi Jinnai,[†,#] Satoshi Koizumi,[||] Kazuya Aizawa,[▽] and Takeji Hashimoto*[,†,∥,○]

Hashimoto Polymer Phasing Project, ERATO, Japan Science and Technology Agency, and Department of Polymer Chemistry, Graduate School of Engineering, Kyoto University, Kyoto 606-8510, Japan, Advanced Science Research Center and Qantum Beam Science Directorate, Japan Atomic Energy Agency, Tokai-mura, Ibaraki 319-195, Japan

Received March 8, 2008; Revised Manuscript Received July 31, 2008

ABSTRACT: Internal structures of the opaque poly(*N*-isopropylacrylamide) gel obtained at the preparation temperature (T_P) higher than 24.5 °C was found to have hierarchical structures by means of a combined small-angle-scattering (CSAS) method of small-angle light scattering (SALS), ultra-small-angle neutron scattering (USANS), and small-angle neutron scattering (SANS) with an aid of laser scanning confocal microscopy (LSCM). The combined CSAS and LSCM studies revealed that a global structure of the gels had a sponge-like two-phase structure. The polymer-rich phase of the sponge was filled with microgels having highly cross-linked network ("tight network") chains that are interconnected by loosely cross-linked network ("loose network") chains swollen with water, while the other phase of the sponge was mostly composed of water. These two phases were cocontinuous in three-dimensional space, hence, forming macroscopic gels. The SALS and USANS studies clarified that the sponge had a characteristic spacing of ≈12 μm and the mass fractal structure characterized by its dimension = 2.5, the upper and lower cutoff lengths were ≈6 and ≈0.5 μm, respectively. The physical meaning of these values is discussed in the text. The SANS studies further revealed the following characteristic parameters about the local structure of the gels: the microgel of diameter ≈ 60 nm; the thermal correlation lengths of the loose and tight network chains ≈ 11 and ≈ 1.2 nm, respectively, though these are averaged values in the range of T_P, 24.5 ≤ T_P (°C) ≤ 38.0. The swelling behavior of the gels was also studied and discussed in light of the sponge-like gel model. The mechanism of the formation of the hierarchical structures was discussed on the basis of the special reaction field where the two-step cross-linking reaction occurs, as detailed in the text.

I. Introduction

In this paper, we aim to report "sponge-like gels" as a unique heterogeneous poly(*N*-isopropylacrylamide) [poly(NIPAAm)] gel prepared at preparation temperatures $T_P \geq 24.5$ °C in water. We will report that the gels prepared here have a cocontinuous sponge-like two-phase structure, one phase composed of a swollen polymer network and the other composed mostly of water, as will be detailed later in this section. A hierarchical structure existing in the heterogeneous gels was characterized by a combined small-angle-scattering (CSAS) method, definition of which will be given in the last paragraph of this section, and laser scanning confocal microscopy (LSCM) method over a wide length scale from ≈1 nm to ≈30 μm. A possible formation mechanism of the intriguing gel structure will be suggested on the basis of a special reaction field in which the gelation reaction occurs.

Chemical gels are versatile materials that commonly consist of a three-dimensionally cross-linked polymer network and a fluid. They have been used as a functional polymer network such as the controlled drug deliveries, sensors, and actuators.[1−4] The network structures influenced by the gelation conditions affect the characteristic properties of the gel such as optical, mechanical, and swelling properties as well as the functions as described above. Boué et al. studied the heterogeneities of polyacrylamide gel by applying the neutron scattering method in relation to the mechanical properties.[5] Although many studies of the gels have been conducted so far,[6−12] there have not been many reports, except for the one,[7] that clarify or visualize the internal structures of the gel at wet state over the wide range of length scale, despite the fact that the internal structures are very important not only to understand the characteristics of the gels but also to design the functions of gels.

After discovery of the volume phase transition of gel,[13] the gels have been recognized as intriguing stimuli-responsive materials. The poly(NIPAAm) gel is one of the most extensively studied thermo-responsive gels because the gel shows the volume phase transition in pure water at 33 °C,[14] when the temperature changes. The optical clarity of the poly(NIPAAm) gel depends on T_P, suggesting the presence of heterogeneities in the gel.[6,7] Therefore, this poly(NIPAAm) gel is considered to provide a good model system for exploring the nature of the heterogeneities of the gels in general.

Rathjen et al. reported the effect of T_P on properties of the poly(NIPAAm) gel.[6] Ju et al.[1] studied the effect of internal microstructures of poly(NIPAAm) gel on controlled drug release characteristics and found that the gel with the heterogeneous internal microstructures showed rapid thermo-responsiveness. Sayil and Okay[8] studied the effect of T_P of poly(NIPAAm) gel on the swelling behavior and then pointed out that the gel

* To whom correspondence should be addressed. E-mail: hashimoto.takeji@jaea.go.jp.
[†] Hashimoto Polymer Phasing Project, Japan Science and Technology Agency.
[‡] Present address: Zeon Corporation, New Business Development Department, 1-6-2 Marunouchi, Chiyoda-ku, Tokyo 100-8246, Japan.
[§] Present address: Zeon Corporation, R&D Center, 1-2-1 Yako, Kawasaki-ku, Kawasaki 210-8246, Japan.
[⊥] Present address: Research & Development Center, Tonen Chemical Corp., 3-1 Chidori, Kawasaki-ku, Kawasaki 210-0865, Japan.
[#] Present address: Department of Polymer Science and Engineering, Kyoto Institute of Technology, Matsugasaki, Kyoto 606-8585, Japan.
[||] Advanced Science Research Center.
[▽] Qantum Beam Science Directorate.
[○] Department of Polymer Chemistry, Kyoto University.

10.1021/ma800518t CCC: $40.75
Published on Web 10/08/2008

prepared at $T_P \geq 22.5$ °C showed the heterogeneities characterized by the existence of more cross-linked and less cross-linked regions. They also reported the condition that creates the macroporous gels after removal of water and revealed that the gels consist of the microspheres by the SEM observation of dried gel.[8] Kara et al. discussed the heterogeneities in the gel network on the basis of transmittance measurements during the formation of poly(NIPAAm) gels.[9] Takata et al.[10,11] investigated the heterogeneities of poly(NIPAAm) gels prepared at various temperatures (5−35 °C). They found that the swelling ratio depends on T_P and that the effective degree of polymerization between cross-linking points increased with increasing T_P.

Those described above are some examples of the studies dealing with the heterogeneities of the poly(NIPAAm) macrogels. Up to now most of the studies focused on the heterogeneities that originate from spatial distributions of cross-linking points in the molecular or local scale less than 100 nm. However, the structural entities of the heterogeneities have not yet been fully clarified. Moreover, the heterogeneities have not yet been studied systematically over a wide length scale, ranging from microscopic to macroscopic length scale.

Along the research line to clarify the structural entities of the heterogeneities over the wide length scale, we studied poly(NIPAAm) gels prepared at $24.5 \leq T_P$ (°C) ≤ 38.0, based on a real-space analysis with LSCM.[7] The LSCM observations elucidated that the heterogeneities owe their origin to an intriguing cocontinuous two-phase sponge-like structure in three-dimensional (3D) space of the gels, comprising the swollen polymer network phase and water phase. More specifically, the polymer network phase consists of the microgels having highly cross-linked networks (defined hereafter "tight networks") and the loosely cross-linked networks (defined hereafter "loose network") interconnecting the microgels.

Although the real-space analysis on the 3D structures of the gels with the LSCM observation gave comprehensible visible images, the information is limited relatively to small local areas of the gels, and hence not necessarily statistically averaged over large areas in a rigorous sense. Moreover, the information is also limited to the length scale larger than 0.2 μm, the spatial resolution limit of the method. In order to quantify the information obtained on the real-space analysis and to gain the missing information at the length scale smaller than 0.2 μm, we further aimed to explore the heterogeneous gel structures on the same specimens with a Fourier-space analysis.

For this purpose, we utilized the CSAS method in this work as a powerful tool to elucidate the 3D structures that are statistically averaged over a large sample volume. The CSAS method employed in this work utilizes small-angle light scattering (SALS), ultra-small-angle neutron scattering (USANS), and small-angle neutron scattering (SANS) in concert to reinforce the pieces of information obtained by each small-angle scattering (SAS) method beyond a level of complementarity. The CSAS method can be applied in situ to the wet gels to study their internal structures over the wide length scale ranging from ≈1 nm to ≈30 μm. The equilibrium swelling behavior as well as optical properties of the gels prepared at different T_Ps was also studied.

II. Experimental Section

II-1. Sample Preparation. *N*-Isopropylacrylamide (NIPPAm) monomer (Tokyo Kasei) was purified by recrystallization from toluene solution into a large amount of *n*-hexane. Ammonium peroxodisulfate (AP; Wako, electrophoresis grade; initiator), *N*,*N*′-methylene-bis(acrylamide) (BIS; Wako, electrophoresis grade; cross-linker), and *N*,*N*,*N*′,*N*′-tetramethylethylenediamine (TEMEDA; Wako, electrophoresis grade; accelerator) were used as received. A monomer solution for gelation was prepared by dissolution of NIPPAm, BIS, and TEMEDA in pure water at 0 °C.

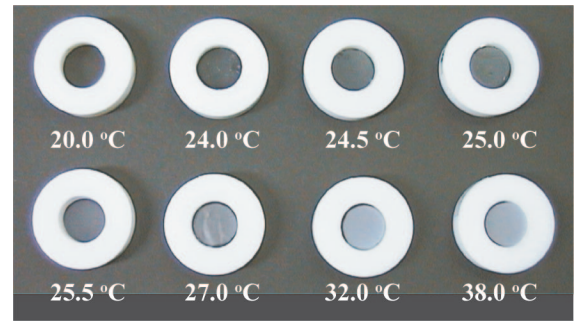

Figure 1. Appearance of the "as-prepared gels in the cell" prepared for a range of preparation temperatures shown in the figure legend but observed at room temperature (23 °C). Outer white rings are the cell holders used for preparation of the gels.

After addition of 0.4 wt % AP aqueous solution to the monomer solution at 0 °C, the mixed solution was quickly introduced into a cell. The cell was assembled with two round glass plates for SALS and light transmission experiments and quarts plates for USANS and SANS experiments (22 mm diameter and 0.17 mm in thickness for both experiments), a ring spacer (18 mm and 22 mm in inner and outer diameters, respectively, 0.1 mm in thickness for light-transmission and SALS experiments and 1.0 mm in thickness for USANS and SANS experiments), and a holder made of poly(tetrafluoroethylene) (PTFE; see Figure 1 to be shown later); the cell was immersed in the water bath controlled at $T_P = 20.0$, 24.0, 24.5, 25.0, 25.5, 27.0, 32.0, and 38.0 °C, at which the gelation was initiated and completed within 1 h. Conversions of NIPAAm were more than 99% for all the gelation systems. The concentrations of NIPPAm, BIS, TEMEDA, and AP were 1.33 M, 10.0 mM, 21.0 mM, and 1.75 mM, respectively. For USANS and SANS measurements, the gel was prepared in heavy water instead of light water to enhance the scattering contrast between the gel network and its medium.

II-2. SALS, USANS, SANS, and LSCM Experiments. All the SALS, USANS, and SANS measurements as well as LSCM observation were performed at a given observation temperature (T_{obs} = 23 °C) on the as-prepared gels enclosed in the same cells in which the gelation took place at the various temperatures, as described in section II-1.[15] A He−Ne laser with wavelength (λ) of 632.8 nm in vacuo was used for SALS measurements. USANS and SANS measurements were performed, respectively, with the PNO spectrometer, which has the Bonse-Hart optics[16−18] and the SANS-J spectrometer[19,20] installed in the JRR-3 Research Reactor, Japan Atomic Energy Agency. The wavelength λ was 0.2 nm for USANS and 0.66 nm for SANS. The distribution of λ, $\Delta\lambda/\lambda = 0.13$ for SANS, where $\Delta\lambda$ is the full width at half-maximum. For the SANS measurement, the distance between the detector and the sample was fixed at 2 and 10 m to cover the wide q range where q will be defined later in eq 1. The data were corrected for background electric noise, empty cell scattering, nonuniformity of detector efficiency, and radially averaged to obtain a data set for scattering intensity profiles with respect to q. USANS profiles were corrected for slit smearing.[21]

SANS profiles were corrected for incoherent scattering. The incoherent scattering intensity for the gels prepared at the various T_Ps should have the same incoherent scattering intensity, because SANS profiles from the gels were measured at the same temperature T_{obs} (=23 °C) and all the gels have the same composition of the same elements. The net incoherent scattering intensity from the gel swollen with D_2O, $I_{gel,inch}$, was estimated on the basis of the incoherent scattering intensity measured for light water (H_2O), $I_{H_2O,inch}$, in the same condition as the SANS measurements for the gels (with the camera length of 2 m) as will be detailed in the references.[22]

LSCM observation was made with LSM 410, Carl-Zeiss, Germany, according to the method detailed in the previous report.[7]

In this work, to survey the hierarchical structures over the wide range of q, CSAS was applied to the gel prepared only at 24.5 °C.

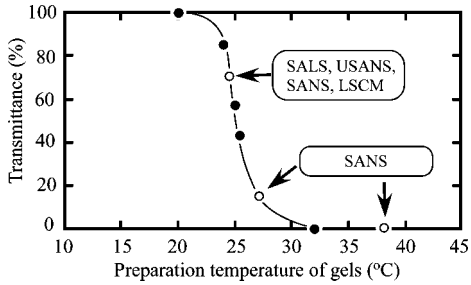

Figure 2. Transmittance of "as-prepared gels in the cell" as a function of preparation temperatures. Open circles designate the gels subjected to further studies with the methods indicated in the legends.

The survey of the hierarchical structures as a function of T_P will be left as future works open to the public. However, the local structures were investigated as a function of T_P by SANS measurements.

II-3. Measurement of Transmittance. The transmittance of the as-prepared gels, which were prepared at T_P from 20.0 to 38.0 °C, was measured with the same cells used for the gelation by means of a UV spectrometer (Shimadzu UV-2500) at $\lambda = 488$ nm and at 23 °C.

II-4. Measurement of Equilibrium Swelling Ratio. Cylindrical gels were prepared at the varying T_Ps in micropipettes having 1.24 mm inner diameter. The gels were taken out from the micropipettes, cut 20 mm long, and then immersed in about 200 cc of deionized water in glass vessels to measure the equilibrium degree of swelling. The glass vessels were held in the temperature controlled water bath at varying T_{obs}s. The diameter of the gels at thermal equilibrium was measured by the observation of the gels in the glass vessels through the optical microscope as a function of T_{obs}. The swelling ratio V/V_0 was calculated by the ratio of diameters of the gels at T_P and after achieving equilibrium swelling, where V_0 and V are the volume of the gel in the respective states as described above.

III. Results

III-1. Appearance of Gels Prepared at Various Temperatures. Figure 1 shows the appearance of the as-prepared poly(NIPAAm) gels enclosed in the same cell used for the gelation at various T_P in the range between 20.0 and 38.0 °C but observed at 23 °C.[15] Because the cell used for preparation of the gels is designed so as to be used also for transmittance measurements, the "as-prepared gels in the cell" were used for the transmittance measurement without taking it out from the cell.[15,23]

The gel prepared at 20.0 °C was quite transparent and the opacity was observed for the gels prepared at $T_P \geq 24.5$ °C. The degree of opacity was increased with T_P. The gels prepared at 32.0 and 38.0 °C were completely turbid at $T_{obs} = 23$ °C. The observed turbidity did not disappear even when T_{obs} was lowered from 23 to 10 °C. On the contrary, the aqueous solution of linear poly(NIPAAm) at 32 and 38 °C, which showed the same turbidity as the gels at the corresponding temperatures, became transparent at low temperatures of 23 and 10 °C. This fact indicates that the opaque gels have heterogeneities permanently fixed in the chemical gelation process.

To quantify a degree of the opacity as an index of heterogeneities of the "as-prepared gels in the cell", transmittance of each gel shown in Figure 1 was measured at 23 °C. Figure 2 shows the thus measured transmittance as a function of T_P. The transmittance of the gels prepared at 20.0 °C was 100%. With the increase in T_P, the transmittance dramatically decreased at around $T_P = 25.0$ °C and eventually went down to zero at $T_P \geq 32.0$ °C, which is close to the lower critical solution temperature (T_{LCST}; 34 °C) of linear poly(NIPAAm) solutions in water having corresponding concentrations (15.1 wt %).[24] Internal structures of the opaque gels prepared at 24.5 °C was further studied with CSAS and LSCM and the turbid gels at 27.0 and 38.0 °C with SANS.

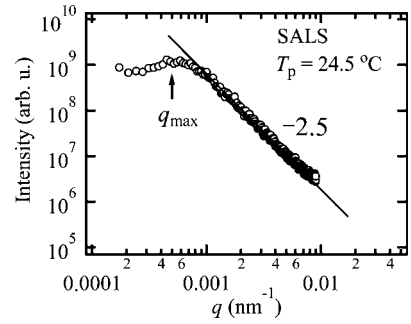

Figure 3. Double logarithmic plot of the SALS scattered intensity as a function of q at 23 °C for the "as-prepared gel in the cell" prepared at 24.5 °C.

III-2. Small-Angle Light Scattering (SALS). SALS measurements were carried out to quantitatively investigate the fine structures in the translucent gels. However, the measurements are rather limited to the gel having relatively high transmittance to avoid complication of the scattering analysis due to multiple scattering. Consequently, among the gels prepared at various T_Ps, the one prepared at 24.5 °C was employed for SALS measurements. The other gels prepared at $T_P \geq 25.0$ °C had the transmittance lower than 60% and, hence, were not suitable for the SALS analysis. From light of LSCM observation, the structures of the gel prepared at 24.5 °C is appeared to be similar to those prepared at $T_P \geq 25.0$ °C with respect to such main features that all the gels have cocontinuous sponge-like two-phase structures: one phase comprises the swollen polymer networks and the other phases are composed mostly of water.[7] Thus the SALS data obtained at 24.5 °C may represent approximately those obtained at $T_P \geq 25.0$ °C.

Figure 3 shows the SALS profile for the gel prepared at 24.5 °C. The scattering intensity profile $I(q)$ showed a maximum at $q = q_{max} \approx 5.0 \times 10^{-4}$ nm^{-1},[25] where q is the magnitude of scattering vector defined by

$$q = (4\pi/\lambda)\sin(\theta/2) \quad (1)$$

with λ and θ being the wavelength of the incident beam and scattering angle both in the medium. The q_{max} originates from the presence of the characteristics length, $d = 2\pi / q_{max} \approx 12$ μm for the internal structures of the gel, which reflects the most probable spacing of the sponge-like two-phase structure described earlier[7] and as will be shown later in Figure 9. The SALS profile in Figure 3 at $q > q_{max}$ showed a straight line with a slope of −2.5 over the q range from 1.0×10^{-3} to 1.0×10^{-2} nm^{-1}, so that scattering obeys a power law,

$$I(q) \sim q^{-\alpha} \quad (2)$$

with the exponent $\alpha = 2.5$. This in turn suggests that the gels may have a fractal structure with mass fractal dimension of 2.5, as will be clearly visualized in section IV later.

III-3. Ultra-Small-Angle Neutron Scattering (USANS). USANS covers almost the same q range as SALS, except for a small extension of a large part of q, ranging from 9×10^{-3} to 2.5×10^{-2}. This small extension in USANS is indispensable for the CSAS method, since this q range could not be covered by SANS at the stage when these experiments were conducted. The USANS profile in Figure 4 showed a maximum at the same $q_{max} \approx 5 \times 10^{-4}$ nm^{-1} as in the SALS profile in Figure 3. The USANS profile at $q > q_{max}$ is also given by eq 2, hence, showing a straight line with a slope of −2.5 up to somewhat larger q value (1.3×10^{-2} nm^{-1}) than the SALS profile. Some scattering of the data around the straight line in the region of $0.001 \leq q$

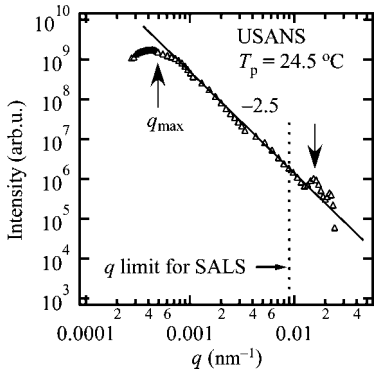

Figure 4. Double logarithmic plots of the USANS profile as a function of q at 23 °C for the "as-prepared gel in the cell" prepared at 24.5 °C.

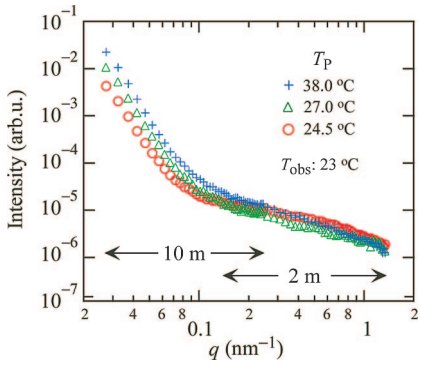

Figure 5. SANS profiles of the "as-prepared gels in the cells" prepared at 24.5, 27.0, and 38.0 °C. All the profiles were measured at 23 °C.

(nm^{-1}) ≤ 0.01 are quite immaterial and lie well within the experimental errors. There is a change in the USANS profile over the q range from 1.3 × 10^{-2} nm^{-1} to 2.5 × 10^{-2} nm^{-1}, the range of which can not be covered by SALS measurement, where the USANS profile tends to show a broad peak or shoulder at $q \approx 0.015$ nm^{-1}, origin of which will be discussed later in section IV-1. Consequently, both the SALS and USANS profiles at q < 1.3 × 10^{-2} nm^{-1} tend to see the same coarse-grained structure of gels, which reflect a spatial distribution of the microgels in water as will be clarified later in section IV-1. It seems that the loose networks interconnecting the microgels are not visible in the q range covered by SALS and USANS, as will be also clarified later in section IV-2.

III-4. Small-Angle Neutron Scattering (SANS). SANS, which covers a range of structures smaller than SALS and USANS, was carried out to investigate the local structures of the heterogeneous gels prepared at $T_P \geq 24.5$ °C. Figure 5 shows the SANS profile of the gel prepared at 24.5, 27.0, and 38.0 °C. The SANS scattering profile seems to consist of at least two parts: the region of q < 0.1 nm^{-1} and the region of q > 0.1 nm^{-1}, irrespective of the T_P of the gel. The intensity at q < 0.1 nm^{-1} systematically increases with T_P. These trends will be quantitatively analyzed and discussed later in section IV-2.

III-5. CSAS Profile. On a common double logarithmic scale, the USANS profile was well superposed with the SALS profile and smoothly connected to the SANS profile, upon shifting these profiles only along the vertical axis. The CSAS profile thus obtained is shown in Figure 6. The superposed SALS and USANS profiles showed the part overlapped each other over a very wide range of q (3 × 10^{-4} < q (nm^{-1}) < 1.0 × 10^{-2}), assuring accuracy of the combined SALS and USANS profiles and revealing also both SALS and USANS capture the same two-phase structure, as described in section III-3, for example,

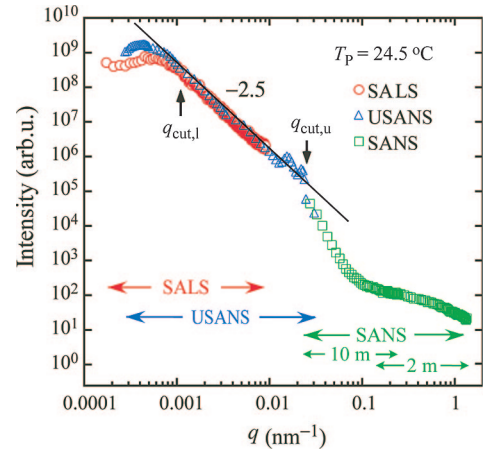

Figure 6. Double logarithmic plot of SALS (red circles), USANS (blue triangles), and SANS (10 and 2 m; green diamonds) scattered intensities as a function of q for the "as-prepared gels in the cell" prepared at 24.5 °C. All the profiles were measured at 23 °C.

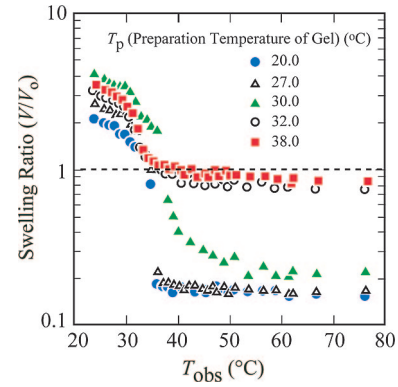

Figure 7. Equilibrium swelling vs T_{obs} of the poly(NIPAAm) gels prepared at various temperatures.

a two-phase structure composed of the spatial distribution of the microgels in the aqueous medium. Consequently, only the absolute intensities are different, but their intensity distributions are almost the same except for a slight difference in the intensities around their broad scattering maximum at $q = 4-5$ × 10^{-4} nm^{-1}. The small extension of the higher q range (9.0 × 10^{-3} < q (nm^{-1}) < 2.5 × 10^{-2}) attained by USANS, which was inaccessible by SALS, turned out to be quite important to obtain the CSAS profile. This is because this extension made it possible to combine the SALS and SANS profiles. The USANS and SANS profiles were combined with good accuracy, because the USANS tail and the SANS head overlap each other over a sufficient q range. The slope of the straight line of the combined SALS and USANS profile is −2.5, and the lower cutoff wavenumber ($q_{cut,l}$) and upper cut off wavenumber ($q_{cut,u}$) are estimated to be 1.0 × 10^{-3} and 1.3 × 10^{-2} nm^{-1}, respectively. The corresponding upper cutoff length $l_{cut,u}$ and lower cutoff length $l_{cut,l}$ are 6.3 μm and 480 nm, respectively (where $l_{cut,J} \equiv 2\pi / q_{cut,J}$, $J = u$ or l).

III-6. Equilibrium Swelling Behavior of the Gels Prepared at Different Temperatures. A series of the equilibrium swelling curves of the gels prepared at different T_P is shown in Figure 7. At low temperatures below the T_{LCST} (34 °C) of the corresponding poly(NIPAAm) aqueous solutions, all the gels swelled more than the original size of the as-prepared gels. On the other hand, at high temperatures above the T_{LCST}, the gels shrank into two states, depending on the T_P of the gels. The gels prepared at the lower temperatures (20.0, 27.0, and 30.0 °C) than the T_{LCST} shrank into the very compact state with the

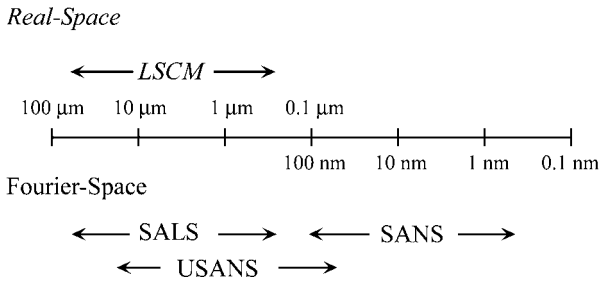

Figure 8. Real-space analysis and Fourier-space analysis employed in this study and the length scale covered by each method.

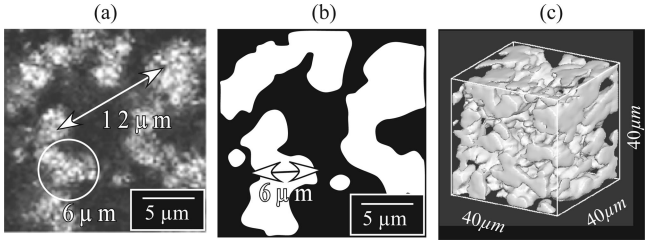

Figure 9. (a) LSCM sliced image of "as-prepared gel in the cell" prepared at 24.5 °C and observed at 23 °C. The length indicated by the arrow corresponds with the spacing (12 μm) obtained from q_{max} in the SALS and USANS scattering profiles. The diameter of the circles indicates the $l_{cut,u}$ ($\approx$6 μm) obtained from $q_{cut,l}$ in SALS and USANS scattering profiles. (b) Binarized image of (a). The arrow indicates the $l_{cut,u}$. (c) 3D image (40 $\times$ 40 $\times$ 40 μm^3) constructed by a series of sliced images, as shown in (b).

swelling ratio equal to 0.18, while the gels prepared at the temperatures (32.0 and 38.0 °C) higher than the T_{LCST} had almost the same size as that of the as-prepared gels.

IV. Discussion

Figure 8 summarizes the length scales that the LSCM and CSAS measurements in the present work can cover for investigation of the internal structures of the gel prepared at 24.5 °C. The real-space information was obtained with the LSCM measurement over the length scale from tens μm to hundreds nm. The Fourier-space information was obtained over the much wider length scale than LSCM, ranging from tens μm to nm. LSCM gives the structural information in the approximately same length scale as SALS and USANS: These real-space and Fourier-space information "in concert" reinforce each other beyond the level of complementarity as each method does. On the other hand, SANS among CSAS specifically cover the gel structures in much smaller length scale, less than 100 nm, which can not be covered by LSCM, SALS, and USANS.

In this section we shall first discuss the global structure of the gels obtained from SALS and USANS along with the LSCM results (section IV-1). We then discuss the local structure of the gels obtained from SANS (section IV-2). Finally, we shall discuss a possible scenario for the special gelation mechanism responsible for formation of the heterogeneous gel structures prepared at $T_P \geq$ 24.5 °C (section IV-3) and add some remarks on the swelling (IV-4) and optical properties (IV-5).

IV-1. Global Structures. Both SALS and USANS showed (i) the scattering maximum at $q_{max} = 5.0 \times 10^{-4}$ nm^{-1} and (ii) the power law given by eq 2, with $\alpha = 2.5$ over the q range from 1.0×10^{-3} nm^{-1} to 1.3×10^{-2} nm^{-1} (Figures 3 and 4, respectively). We shall interpret below the data obtained in Fourier-space with an aid of the data obtained in real-space.

Figure 9 shows an LSCM sliced image (part a), its binarized image (part b), and 3D binarized image (part c) of the gel prepared at 24.5 °C.[7,26] Figure 9a shows regions rich in bright spots dispersed in the dark featureless medium. We found that these regions are continuous in 3D space, being interconnected beneath and above this slice, when we trace them over the consecutive slices along the depth (or the incident beam) direction. We believe that the image contrast owes its origin to the scattering, that is, the scattering from the small "structural entities" make them appear as the bright spots. The spatial brightness distribution in the sliced image should reflect a spatial distribution and, hence, concentration fluctuations of the structural entities within the volume of the slice.

The binarized image in Figure 9b then presents a coarse-grained image of Figure 9a that consists of two phases: one phase consists of the phase rich in the small structural entities (bright phase) and another consists of the featureless water phase (dark phase). Moreover, the 3D image in Figure 9c reveals that the two phases are cocontinuous in 3D space, having characteristics similar to the sponge-like structures found in binary phase-separated liquid mixtures.[27−32]

The intriguing sponge-like gel model qualitatively visualized by LSCM, under the limitations as described in section I, can now be quantified firmly by SALS and USANS. The $q_{max} = 5.0 \times 10^{-4}$ nm^{-1} in SALS and USANS corresponds with the characteristic length (spacing = 12 μm; most probable spacing) of the sponge-like two-phase structure shown in Figure 9c. This spacing, resulting from the phase-separating structure pinned at the second-stage cross-linking reaction, as will be elaborated later in section IV-2, is well consistent with the spacing observed in the LSCM, as demonstrated in Figure 9a.

In the bright phase of the sponge-like two-phase structure shown in Figure 9b,c, the small scattering (or structural) entities are anticipated to be distributed, as observed in Figure 9a, with a mass fractal structure with the dimension $d_m = \alpha = 2.5$ (see eq 2). The upper cutoff length $l_{cut,u} = 2\pi/q_{cut,l} \cong 6$ μm is also well consistent with the characteristic length (the most probable length) of the cross-sections of the bright sponge phase, as demonstrated by a circle of 6 μm diameter in Figure 9a and by the arrow in Figure 9b. The lower cutoff length of the mass fractal structure, $l_{cut,l} = 2\pi/q_{cut,u} \cong 0.5$ μm, should be intimately related to the small bright structural entities that are designated "microgels", as will be elaborated in the next section (IV-2). The fractal dimension of $d_m = 2.5$ for the centers-of-mass distribution of the microgels reveals that the microgels associate themselves, driven by the diffusion-limited aggregation, into the bright phase of the sponge-like structure, which eventually pinned by the cross-linking, as will be elaborated also in the following sections (sections IV-2 and IV-3).

The broad peak or shoulder at $q \approx 0.015$ nm^{-1} is reproducible and attributed to an intermicrogels interference effect on the scattering from the microgels. The maximum may be predicted through the radial distribution function of the centers of mass of the microgels on the basis of the Percus−Yevick's hard sphere model[33] or more simply the Debye's hard sphere model.[34]

IV-2. Local Structures as Elucidated by SANS. In this part, we shall present an analysis of the SANS profiles with an aid of the pieces of information obtained from the global structural analysis discussed in the previous section. Figure 10 shows an LSCM sliced image (part a), the enlarged image of the region encompassed by the white circle in part a that focuses on a region dense in the small structural entities (part b), and a schematic illustration of the part encompassed by the black circle in Figure 10b (part c). Here we assume that the small structural entities are "microgels" having the tight networks and that the microgels themselves are interconnected with the loose networks, as schematically illustrated in Figure 10c, throughout the polymer network rich phase (bright phase in Figure 9c). The latter assumption is justified by the macroscopic nonfluidity of the gel.

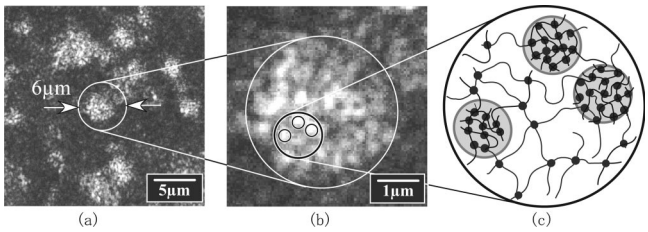

Figure 10. (a) Sliced LSCM image of "as-prepared gel in the cell" prepared at 24.5 °C. (b) Zoom-in view of (a). (c) Schematic illustration of local gel structures.

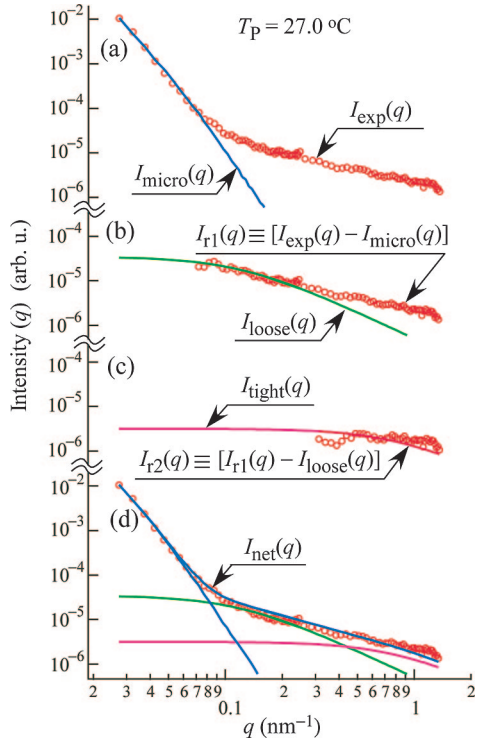

Figure 11. Decomposition of the experimental SANS profile $I_{exp}(q)$ into the three contributions, $I_{micro}(q)$, $I_{loose}(q)$, and $I_{tight}(q)$.

To verify the local model shown in Figure 10c, the SANS profiles shown in Figure 5 were analyzed. It should be noted that phase rich in bright spots in Figure 10a,b highlights the local structure of the polymer-rich phase (the bright phase) of the sponge-like structures shown in Figure 9b,c.

Based on the pieces of information given above by the real-space observation, we can now visualize the local structure of gels as an assembly of (i) the microgels having the tight networks with thermal correlation length ξ_{tight}, (ii) the loose networks having thermal correlation length ξ_{loose}, which interconnect the microgels, and (iii) the microgels with their centers of mass undergoing Brownian motion with thermal correlation length Ξ. Ξ should correspond with the lower cutoff length $l_{cut,l}$ for the mass fractal structure elucidated in section IV-1. SANS can provide all these pieces of information about the local structures and dynamics as detailed below.

A. Theoretical Background for SANS Analysis. The thermal concentration fluctuations of the tight networks within the microgel will give rise to the scattering $I_{tight}(q)$ given by Ornstein−Zernike (OZ)[35]

$$I_{tight}(q) = k_{tight}(1 + q^2\xi_{tight}^2)^{-1} \tag{3}$$

where k_{tight} is a proportionality constant that depends on ξ_{tight} and the concentration of the tight-network chains in the microgels. The thermal concentration fluctuations of the loose networks will give rise to another OZ scattering

$$I_{loose}(q) = k_{loose}(1 + q^2\xi_{loose}^2)^{-1} \tag{4}$$

where k_{loose} is a proportionality constant which depends on ξ_{loose} and the concentration of the loose network chains in the network-rich (or the bright) phase.

The correlation function $\Gamma_{micro}(r)$ for thermal concentration fluctuations of the microgel themselves should be given by the convolution product of a correlation function $\Gamma_{therm}(r)$ for the thermal concentration fluctuations for the centers-of-mass of microgels and the correlation function for the shape of the microgels $\Gamma_{shape}(r)$

$$\Gamma_{micro}(r) = \Gamma_{therm}(r) * \Gamma_{shape}(r) \tag{5}$$

where the symbol $*$ designates convolution product and $\Gamma_{therm}(r)$ is given by

$$\Gamma_{therm}(r) \propto \frac{1}{r}\exp\left(\frac{-r}{\Xi}\right) \tag{6}$$

Consequently scattering $I_{micro}(q)$ from the microgels undergoing Brownian motions is given from eq 5 by

$$I_{micro}(q) = k_{micro}\,\mathcal{F}\{\Gamma_{therm}(r)\}\,\mathcal{F}\{\Gamma_{shape}(r)\} = k_{micro}(1 + q^2\Xi^2)^{-1}F(q) \tag{7}$$

where $\mathcal{F}\{X\}$ denotes Fourier transformation of X, $F(q)$ is the form factor of the microgels, and k_{micro} is a proportionality constant that depends on Ξ and concentration of the microgels in the network-rich phase. We note that $\mathcal{F}\{\Gamma_{therm}(r)\}$ gives rise to the OZ function of the first term in the second line of right-hand side of eq 7.[36] It is reasonable to assume that the microgel is a sphere of radius R, then $F(q)$ is given by

$$F(q;R) = \left[\frac{4\pi R^3}{3}\frac{3}{u^3}(3\sin u - u\cos u)\right]^2, \quad u \equiv qR \tag{8}$$

When there is a size distribution for the microgels given by normalized distribution function of $P(R)$, $F(q)$ is given by

$$F(q) \sim \int_0^\infty P(R)F(q;R)\mathrm{d}R \tag{9}$$

It is well expected that the characteristic lengths relevant to the local structures are quite different, satisfying $\Xi > \xi_{loose} > \xi_{tight}$. If this is the case, the contribution of the scattering from each local structural element to the net scattering $I_{net}(q)$ is well separated, so that $I_{net}(q)$ is approximated by a weighted average of each contribution

$$I_{net}(q) = f_{micro}(1 + q^2\Xi^2)^{-1}F(q) + f_{loose}(1 + q^2\xi_{loose}^2)^{-1} + f_{tight}(1 + q^2\xi_{tight}^2)^{-1} \tag{10}$$

with the respective weighting factors satisfying[37]

$$f_{micro} + f_{loose} + f_{tight} = 1 \tag{11}$$

In this work, we assume that $P(R)$ is given by the log-normal distribution,

$$P(R) = \frac{1}{R\sigma\sqrt{2\pi}}\exp\left(-\frac{|\ln R - \mu|^2}{2\sigma^2}\right) \tag{12}$$

where mean radius $<R>$ and variance σ_R^2 of $P(R)$ are given by

$$<R> \equiv \exp[\mu + (\sigma^2/2)], \quad \sigma_R^2 \equiv [(\exp\sigma^2) - 1]\exp(2\mu + \sigma^2) \tag{13}$$

B. Analysis of SANS Profiles. We attempted to fit the experimental SANS profiles shown in Figure 5 with the predicted profiles given by eqs 3, 4, and 7−12 according to the following procedures as demonstrated by Figure 11. We first

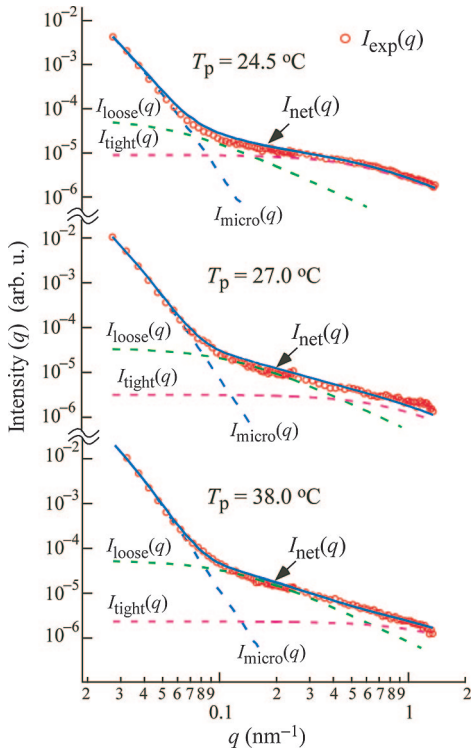

Figure 12. Prediction of experimental SANS scattering profile, $I_{exp}(q)$, with respect to the three terms $I_{micro}(q)$, $I_{loose}(q)$, and $I_{tight}(q)$ on the basis of the proposed local structure of the gels shown in Figure 10.

fitted a part of the experimental scattering profile $I_{exp}(q)$ at the lowest q range ($q < 0.07$ nm^{-1}) with the predicted profile $I_{micro}(q)$ obtained by eqs 7−9, 12, and 13, where the fitting parameters, Ξ, $<R>$, and σ_R determine the q dependence of $I_{micro}(q)$ and k_{micro} determines the intensity level (part *a*). We then subtracted $I_{micro}(q)$ from $I_{exp}(q)$ to obtain $I_{r1}(q) \equiv I_{exp}(q) - I_{micro}(q) = I_{loose}(q) + I_{tight}(q)$. Then a part of the profile $I_{r1}(q)$ at the low q range ($q < 0.2$ nm^{-1}) was fitted with the predicted profile $I_{loose}(q)$ obtained by eq 4, where the fitting parameter ξ_{loose} determines the q dependence and k_{loose} determines the intensity level (part *b*). The residual scattering intensity $I_{r2} \equiv I_{r1}(q) - I_{loose}(q) = I_{tight}(q)$ was fitted with the predicted profile $I_{tight}(q)$ given by eq 3, where the fitting parameter ξ_{tight} determines the q-dependence and k_{tight} determines the intensity level (part *c*). The above three steps of the fitting procedure was repeated until the best fit was obtained between the predicted profile $I_{net}(q)$ and the experimental profile $I_{exp}(q)$ (part d). According to this analytical procedure, the errors caused by the estimation of $I_{micro}(q)$ and $I_{loose}(q)$ are accumulated on the errors for the estimation of $I_{tight}(q)$. Hence, it should be noted that the accuracy of the analysis decreases in the order of $I_{micro}(q)$, $I_{loose}(q)$, and $I_{tight}(q)$.

Figure 12 shows the best-fitted results between the experimental (circles) and predicted (solid line) profiles for the gels prepared at T_P = 24.5, 27.0, and 38.0 °C, where dashed lines marked by $I_{micro}(q)$, $I_{loose}(q)$, and $I_{tight}(q)$, represent, respectively, the contributions of the first to the third term in eq 10 to the net predicted scattering profile (solid line). In the real fitting process, it is important to note that the value Ξ should be approximately equal to the lower cutoff length $l_{cut,l}$ ($\cong$500 nm as evaluated from the upper cutoff wavenumber $q_{cut,u}$ in Figure 6) of the mass fractal structure, so that $q\Xi \cong ql_{cut,u} = 13.5-650$, hence, $q^2\Xi^2 \gg 1$, for the q range covered by SANS ($2.7 \times 10^{-2} < q$ (nm^{-1}) < 1.3). Consequently, eq 7 is well approximately given by $q^{-2}F(q)$. It should be noted that $I_{micro}(q) \sim q^{-6}$ in the high q limit of $q \geq 0.06$ nm^{-1}, because in this limit $F(q) \sim q^{-4}$. The observed SANS profiles are found to be well predicted on the basis of the proposed model on the local structures of the gels as schematically demonstrated by Figure 10c.

The parameters characterizing the local structure of the gels are summarized in Table 1, and the estimated distribution functions $P(R)$ employed are represented in Figure 13. It is worth noting here that the estimated weighting factors f_{micro}, f_{loose}, and f_{tight} in Table 1 are still apparent weighting factors because they respectively depend on the concentration of the microgels (ϕ_{micro}), the concentration of the loose network chains and the correlation length (ϕ_{loose} and ξ_{loose}), and the concentration of the tight network chains and the correlation length (ϕ_{tight} and ξ_{tight}). Consequently, further analyses are required to extract the true weighting factors. Therefore, at this stage, we like to focus only on the quantities $<R>$, σ_R, ξ_{loose}, and ξ_{tight} in Table 1, which can be estimated only from the relative scattering intensity distributions with respect to q. It should be kept in mind that ξ_{tight} suffers from relatively larger errors compared with other parameters.

The results on these parameters revealed a systematic change with increasing T_P, as follows: (1) The average radius $<R>$ of the microgels and their size distribution parameter σ_R increase as shown in Table 1 and Figure 13, but (2) the thermal correlation lengths of the loose network ξ_{loose} and the tight networks in the microgel ξ_{tight} decrease, as shown in Table 1. We believe these trends are reasonable from the viewpoint that the amplitude of thermal concentration fluctuations of poly(NIPAAm) before cross-linking increases with T_P, which in turn may give (i) a greater thermodynamic driving force for the microgels formation, hence, accounting for a larger $<R>$ and σ_R, (ii) a higher cross-linking density in the microgels, hence, accounting for a smaller ξ_{tight}, and (iii) higher cross-linking density of the loose network chains, hence, accounting for a smaller ξ_{loose}.

It is interesting to note that the value $2<R>$ ($\approx$60 nm) for the average diameter of the microgels is much smaller than that observed by LSCM ($\approx$300 nm). This fact may be attributed partly to the Brownian motion of the microgels during the data acquisition time required for the LSCM imaging, which may cause the size observed by LSCM larger and partly to the resolution limit of the LSCM (0.2 μm), which smears the microgels, hence, causing the apparent size observed by LSCM larger. The thermal correlation length ξ_{loose} for the loose networks connecting the microgels is large ($\approx$17 nm) at 24.5 °C,[38,39] which may reflect cross-linking between the microgels undergoing Brownian motion and poly(NPAAm) chains dissolved in the medium which are expected to have a low concentration. As T_P increases, ξ_{loose} systematically decreases, which is also reasonable in light of the microgels and dissolved poly(NIPAAm) chains being more dense in one of the phase (the bright phase in Figure 9b,c) rich in poly(NIPAAm) before the "second-step cross-linking process", which will be postulated and discussed later in section IV-3.

Based on the SANS results as summarized in Table 1, we can now visualize the local structure of the gels, comprising the microgels having the tight network chains and the loose network chains interconnecting the microgels, as schematically shown in Figure 14(b-2). The other parts of (a-1), (a-2), and (b-1) in Figure 14 will be discussed in the next section. The values $<2R> \approx 50$ nm, $\xi_{loose} \approx 17$ nm, and $\xi_{tight} \approx 1.7$ nm in the figure are the values of the gels prepared at T_P = 24.5 °C. The value, $\approx$500 nm, was the value at T_P = 24.5 °C obtained from USANS. In the next section, we shall discuss a possible model for the gelation process leading to the heterogeneous gel structure.

IV-3. Possible Scenario for Reaction-Induced Heterogeneous Gelation Process. In this section we shall present a possible scenario for the heterogeneous gelation process at $T_P \geq$ 24.5 °C.

Table 1. Summary of the Characteristic Scattering Parameters Reduced from SANS

parameters T_P (°C)	f_{micro}	f_{loose}	f_{tight}	$<R>$ (nm)	σ_R	ξ_{loose} (nm)	ξ_{tight} (nm)
24.5	4.6×10^{-13}	0.87	0.13	25.7	16.6	17 ± 2.1	1.7 ± 0.03
27.0	1.8×10^{-12}	0.92	0.08	30.0	17.9	8.3 ± 0.54	1.2 ± 0.06
38.0	1.4×10^{-12}	0.96	0.04	38.2	20.4	8.1 ± 0.79	0.7 ± 0.7

The process seems to involve the reaction in the specific reaction fields, that have not been paid much attention so far.

From a point of view of the reaction rate, the cross-linker is expected to be incorporated statistically randomly[40] along the resultant copolymer chain with its mole fraction of 7.5×10^{-3}. Concerning the reaction-induced heterogeneous gelation, it is important to note the following features: (i) The copolymerization reaction is quite rapid, so that linear chains with an average degree of polymerization (DP), $N \approx 3 \times 10^3$, will be rapidly formed, as expected from the report by Kubota et al.;[39] (ii) however, concentration of the polymers, ϕ_P, gradually increases with time, up to the volume concentration of $\phi_p \approx 0.17$ at 100% monomer conversion;[41,42] and (iii) the cross-linking reaction is supposed to be a rather slow process because of steric hindrance of the bulky copolymer chains.

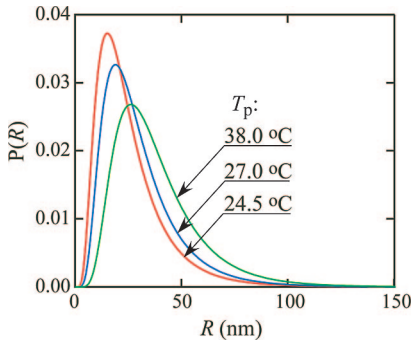

Figure 13. Estimated normalized distribution of the radius R of the microgels prepared at the three preparation temperatures.

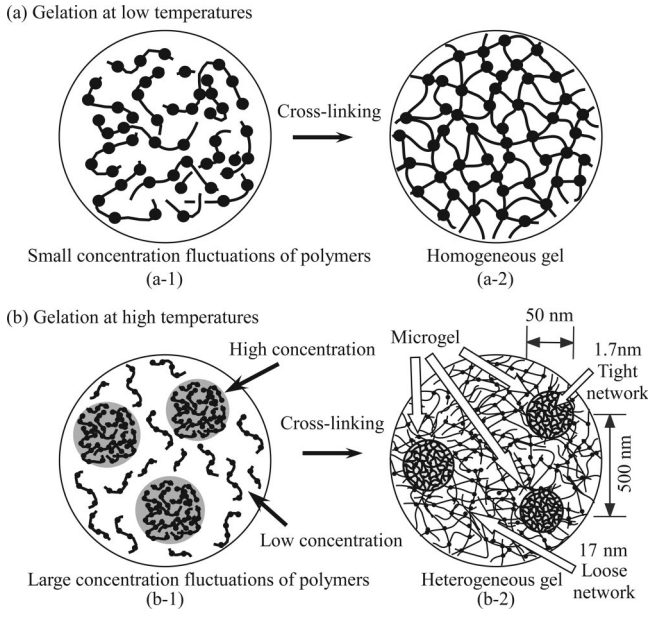

Figure 14. Schematic diagram showing the gelation process at two typical preparation temperatures. (a) Gelation at lower temperatures than the T_{LCST} and (b) at higher temperatures than the T_{LCST}. (b-2) shows a model for the local structure of the heterogeneous gel obtained at 24.5 °C, which are drawn from the analysis of SANS data shown in Table 1. This local structure model is composed of the microgels, which have diameter $<2R> \approx 50$ nm, and the tight networks chains with $\xi_{tight} \approx 1.7$ nm and the loose network chains with $\xi_{loose} \approx 17$ nm, which interconnect the microgels.

Consequently, in the reaction system, the rapidly grown large molecular weight copolymers with the cross-linkers, slowly increases its concentration ϕ_p with time. The cross-linking reaction may occur under the special reaction field where the large thermal concentration fluctuations of the polymers exist or even liquid−liquid phase-separation occurs in the reacting solution at high T_Ps.

At the low T_P (e.g., 20.0 and 24.0 °C), the attractive interactions of the hydrophilic groups (amide groups) of the polymers and water win the repulsive interactions of hydrophobic groups of the polymers (such as isopropyl and methylene groups) and water. Thus, the increasing number of polymers created by the reaction keep forming a thermodynamically stable solution, giving rise to small concentration fluctuations of the polymer as schematically shown in Figure 14(a-1), which in turn causes homogeneous cross-linking reaction; thereby, the system ends up to a more or less homogeneous gel as schematically illustrated in Figure 14(a-2).

On the other hand, at the high T_Ps (e.g., from 24.5 to 38.0 °C), the repulsive interactions may increasingly important relatively to the attractive interactions with increasing T_P, giving rise to an increasing positive value of χ (thermodynamic interaction parameter between the polymer segments and water). Consequently, upon increasing ϕ_P, the reaction solution generates large concentration fluctuations or phase separation, giving rise to regions rich in polymer and those poor in polymers, as schematically shown in Figure 14(b-1).

It is important to note that the cross-linking reaction at $T_P \geq 24.5$ °C occurs in a special reaction field, which involves a coupling between the chemical reaction and such physical events as the thermal concentration fluctuations or even the "viscoelastic phase separation" (specifically in the case of $T_P = 38.0$ °C).[43,44] The rate of the cross-linking reaction in polymer-rich regions should be obviously faster than that in polymer-poor regions. Consequently, the cross-linking may occur selectively in polymer-rich regions, which may result in the creation of the microgels having tight network chains in the polymer-poor matrix solution. It is expected that the local cross-linking will promote formation of the microgels. We define this cross-linking reaction as "the first-step cross-linking reaction".

The created microgels undergoing Brownian motion coexist with the (as-created and/or newly created) polymers dissolved in the medium. Then the microgels and the polymer dissolved in water will provide another special reaction field for the cross-linking reaction, which is defined hereafter as "the second-step cross-linking reaction". During the second-step cross-linking reaction, the phase separation into the so-called "sponge-like cocontinuous two-phase structures" may be developed through viscoelastic phase separation, when the T_Ps are sufficiently high. This second-step cross-linking reaction will form loose networks interconnecting the microgels in one of the two phases, which is rich in the microgels and dissolved polymers, so that the macroscopically cross-linked network is eventually constructed. The first-step and second-step cross-linking reactions fix the local structure of the gels [Figure 14(b-2)]. The second-step cross-linking reaction will fix also the growth of the phase-separating structure and, hence, the higher-order structure of the gels (Figure 9a−c).

IV-4. Equilibrium Swelling Behavior. The poly(NIPAAm) gels prepared at T_Ps ranging from 20.0 to 38.0 °C showed the different equilibrium swelling behavior as a function of the

Table 2. Swelling Ratio (V/V_0) and Volume Fraction (ϕ_{water}) of Water in the Gels[a]

		preparation temperature(T_P; °C)				
T_{obs} (°C)	swelling characteristics	20.0	27.0	30.0	32.0	38.0
50	V/V_0	0.167	0.175	0.272	0.785	0.908
	ϕ_{water}	<0.01	<0.01	0.38	0.78	0.81
40	V/V_0	0.168	0.175	0.392	0.815	0.978
	ϕ_{water}	0.012	0.029	0.57	0.79	0.83
23	V/V_0	2.13	2.64	4.09	3.14	3.56
	ϕ_{water}	0.92	0.94	0.96	0.95	0.95

[a] Prepared at various temperatures, T_Ps, and at various observation temperatures, T_{obs}s.

observation temperature, T_{obs}, of the gels, as shown in Figure 7. The gels prepared at $T_P \leq 30$ °C change their volume reversibly between the swollen and the shrunken states with respect to the size of the as-prepared gel, when T_{obs} is varied across T_P. On the other hand, the gels prepared at $T_P > 30.0$ °C, for example, 32.0 and 38.0 °C, changed their volume between the swollen state and the state close to the original size of the as-prepared gel.

Table 2 summarizes the volume fraction of water, ϕ_{water}, in the gels, which depends on both T_P and T_{obs}. At $T_{obs} = 23$ °C, all the gels showed the value $\phi_{water} > 0.9$ (or a large swelling ratio of $V/V_0 > 2$), irrespective of T_P, that is, independent of the heterogeneities of the gels, indicating that the loose networks in the heterogeneous gels [shown in Figure 14(b-2)] contribute to the large V/V_0 as those in the homogeneous gel networks shown in Figure 14(a-2) do. More precisely, the V/V_0 at $T_{obs} = 23$ °C increases with T_P to a maximum value at $T_P \cong 30.0$ °C and then decreases with a further increase of T_P, the trend of which is consistent with the earlier report.[11] On the other hand, at $T_{obs} \geq 40$ °C, the gels prepared at $T_P \leq 27.0$ °C had the very low ϕ_{water} (less than 0.03; a small value of $V/V_0 \approx 0.17$), whereas the gels prepared at $T_P \geq 32.0$ °C showed the rather high value ϕ_{water} (over 0.78; V/V_0 close to 1). Thus, the gels showed the different swelling and deswelling behaviors depending on the heterogeneities. The difference in the swelling and deswelling behaviors is rationally interpreted as follows in light of the "sponge-like-gel" model elucidated in sections IV-1 and IV-2.

When T_{obs} is lowered below T_{LCST} for each gel prepared at $T_P \geq 32$ °C, the tight and loose network chains tend to be swollen by water, although the degree of swelling is lower for the tight networks than for the loose networks. Hence, the polymer-rich sponge phase is swollen with lowering T_{obs} below T_{LCST}. This in turn causes the increasing swelling ratio of the as-prepared macroscopic gels as shown in Figure 7, because the sponge phase has a 3D continuity in the macroscopic gels. On the contrary, when T_{obs} is raised above T_{LCST}, the tight and loose networks tend to deswell, though a degree of deswelling is smaller in the tight networks than in the loose networks. This accounts for the shrunken states observed for the as-prepared gels at $24.5 \leq T_P$ (°C) ≤ 30.0. However, the microgels and the loose networks prepared at $T_P = 32.0$ and 38.0 °C may be dehydrated extensively in the gelation process, so that the almost dehydrated microgels are closely packed in the medium composed of the loose network in the polymer-rich sponge phase. Hence, the gels prepared at $T_P \geq 32$ °C cannot go into the shrunken state at $T_{obs} > T_{LCST}$.

Furthermore, when the gel was taken out from the water, an interesting difference was observed in the syneresis behavior. The homogeneous swollen gels prepared at $T_P = 20.0 \sim 24.0$ °C and the swollen sponge-like gels prepared at the low temperature, $T_P = 24.5 \sim 27.0$ °C, did not release the water from the gels. On the contrary, the swollen sponge-like gels prepared at the high temperatures, $T_P = 32.0 \sim 38.0$ °C, loosed water by themselves from the gels, due to the gravitational force. ϕ_{water} in these swollen heterogeneous gels is estimated to be ≈ 0.95 at 23 °C, and the lost water fraction due to the syneresis behavior was estimated to be ≈ 0.11. The rest of water fraction ≈ 0.84 is trapped in the gels.

The intrinsic difference in the swelling behavior of those gels was clarified also by loading a weight on the gels: The homogeneous swollen gels prepared at $T_P = 20.0 \sim 24.0$ °C and the swollen sponge-like gels prepared at $T_P = 24.5 \sim 27.0$ °C did not release the water at all on loading, whereas the sponge-like gels prepared at $T_P = 32.0 \sim 38.0$ °C released the amount of water that depended on the loading weight. This intriguing characteristic observed for the heterogeneous gels prepared at $T_P = 32.0 \sim 38.0$ °C may originate from the heterogeneities in the large length scale. Judging from the difference in the syneresis behavior, the details of the heterogeneous structures of the gels prepared at $24.5 \leq T_P$ (°C) ≤ 27.0 must be different from those prepared at $32.0 \leq T_P$ (°C) ≤ 38.0, though only the gels prepared at 24.5 °C were elucidated in this work. Therefore, to clarify the important difference deserves future work.

IV-5. Optical Properties. The optical properties of the gels can be well controlled by changing T_P as shown in Figures 1 and 2. Moreover, the change in the optical properties with T_P is well interpreted in light of the combined CSAS and LSCM analysis. As T_P increases above 24.5 °C, the microgels become bigger in size and tend to be more tightly cross-linked, hence, becoming denser or more dehydrated as clarified from the change in $\langle R \rangle$ and ξ_{tight} with T_P estimated from SANS (Table 1). With increasing T_P, the microgels are more compactly packed in the polymer-rich phase of the sponge-like structures, as expected from the change in ξ_{loose} (Table 1) and the equilibrium swelling ratio as a function of T_{obs} (Figure 7). These results imply an increasing refractive index difference between the microgels and the aqueous medium and between the two phases in the sponge structure. This fact in turn increases light scattering intensity and, hence, opacity or turbidity.

V. Conclusions

We elucidated that the poly(NIPAAm) gels prepared at $T_P \geq 24.5$ °C have the static heterogeneities characterized by the cocontinuous sponge-like two-phase structure in 3D space where one of the phases of the sponge is composed of swollen network phase and the other phase is composed mostly of water. More specifically, the swollen network phase has the mass fractal structure of the microgels, as a building block of the fractal structure, which have tight network chains and which are interconnected by the loose network chains.

The origin of the hierarchical heterogeneities is proposed to originate from a special reaction field where the cross-linking reaction takes place in the reaction field involving thermal concentration fluctuations or viscoelastic phase separation. The cross-linking in the special reaction field creates first the microgels having tightly cross-linked networks (the first-step cross-linking). Then microgels and a low concentration of the polymers dissolved in the medium undergo the viscoelastic phase separation into two phases. In this stage, the second-step

cross-linking reaction takes place, which interconnects the microgels with loose networks, hence, giving rise to the macroscopic gelation into the sponge-like gels. Based on the intriguing heterogeneous gelation mechanism, we may be able to further develop methods for fine and more precise control of the two-step cross-linking process toward the advance functional network materials. This may well deserve future works in fundamental macromolecular science.

In this work, the hierarchical structures of the heterogeneous gels were explored by the CSAS method only at $T_P = 24.5$ °C. It is very important to clarify how the hierarchical structures depend on T_p, which will deserve future works open to the public.

Acknowledgment. The authors gratefully acknowledge Dr. François Boué for interest and stimulating discussions on this work.

References and Notes

(1) Ju, X. J.; Chu, L. Y.; Zhu, X. L.; Hu, L.; Song, H.; Chen, W. M. *Smart Mater. Struct.* **2006**, *15*, 1767–1774.
(2) Dong, L. C.; Hoffman, A. S. *J. Controlled Release* **1986**, *4*, 223.
(3) Feitas, R. F. S.; Cussler, E. L. *Chem. Eng. Sci.* **1987**, *42*, 97.
(4) Bae, Y. H.; Okano, T.; Kim, S. W. *Makromol. Chem. Rapid Commun.* **1988**, *9*, 185.
(5) Benguigui, L.; Boué, F. *Eur. Phys. J.* **1999**, *B 11*, 439.
(6) Rathjen, M. C.; Park, C.-H.; Goodrich, R. P. *Polym. Gels Networks* **1995**, *3*, 101.
(7) Hirokawa, Y.; Jinnai, H.; Nishikawa, Y.; Okamoto, T.; Hashimoto, T. *Macromolecules* **1999**, *32*, 7093–7099.
(8) Sayil, C.; Okay, O. *Polymer* **2001**, *42*, 7639.
(9) Kara, S.; Okay, O.; Pekcan, O. *J. Appl. Polym. Sci.* **2002**, *86*, 3589.
(10) Takata, S.; Norisuye, T.; Shibayama, M. *Macromolecules* **2002**, *35*, 4779.
(11) Takata, S.; Suzuki, K.; Norisuye, T.; Shibayama, M. *Polymer* **2002**, *43*, 3101.
(12) Shibayama, M.; Isono, K.; Okabe, S.; Karino, T.; Nagao, M. *Macromolecules* **2004**, *37*, 2909.
(13) Tanaka, T. *Phys. Rev. Lett.* **1978**, *40*, 820.
(14) Hirokawa, Y.; Tanaka, T.; Sato, E. *J. Chem. Phys.* **1984**, *81*, 6379.
(15) The difference in the observation and preparation temperatures may generally cause the change in local structure of the gels in terms of a relative volume ratio of network-rich and network-sparse phases, if such network heterogeneities were present, due to local swelling of the network-rich phase on lowering the temperature from T_P or deswelling of the phase on raising the temperature from T_P, although the macroscopic volume of the gel is conserved.
(16) Bonse, U.; Hart, M. *Appl. Phys. Lett.* **1965**, *7*, 238.
(17) Aizawa, K.; Tomimatzu, H. *Physica B* **1995**, *21*, 3214–884.
(18) Yamaguchi, D.; Koizumi, S.; Motokawa, R.; Kumada, T.; Aizawa, K.; Hashimoto, T. *Physica B* **2006**, *385* (386), 1190.
(19) Koizumi, S.; Iwase, H.; Suzuki, J.; Oku, T.; Motokawa, R.; Sasao, H.; Tanaka, H.; Yamaguchi, D.; Shimizu, H. M.; Hashimoto, T. *Physica B* **2006**, *385*−*386*, 1000.
(20) Koizumi, S.; Iwase, H.; Suzuki, J.; Oku, T.; Motokawa, R.; Sasao, H.; Tanaka, H.; Yamaguchi, D.; Shimizu, H. M.; Hashimoto, T. *J. Appl. Crystallogr.* **2007**, *40*, 5474.
(21) Schmidt, P. W. *Acta Crystallogr.* **1965**, *19*, 938.
(22) The incoherent scattering from the gel as a whole $I_{gel,inch}$ was estimated from the incoherent scattering from light water measured under the same conditions as SANS measurements of the gels, $I_{H_2O,inch}$,obs, by using the following conversion factor C, $I_{gel,inch} = C\, I_{H_2O,inch}$,obs. The conversion factor C is a product of the following calculated ratios R_{gel}, R_c, and R_{H_2O}, where $R_{gel} = I_{gel,inch}/I_{H,inch,gel} = 1.32$ (ratio of the incoherent scattering of the gel as a whole to that of H atoms in the gel), $R_c = 0.135$ (ratio of concentration of H atoms in the gel to that of H atoms in H_2O), and $R_{H_2O} = 0.9999$ (ratio of incoherent scattering of one H atom to that of one H_2O molecule. $C = R_{gel}R_cR_{H_2O} = 0.178$.
(23) The gels at T_{obs} has the same macroscopic volume as those at T_P. Hence, the transmittance of the gels at T_{obs} may be approximately equal to that at T_P.
(24) Unpublished data.
(25) The q_{max} was found to be independent of T_P ($24.5 \le T_P$ (°C) ≤ 38.0), from the FFT analysis of the LSCM images, observed at 23 °C, for the as-prepared gels obtained at different T_Ps. This fact appears to imply that the most probable spacing of the sponge-like structure, created through the phase-separation and the pinning (of the phase-separating structure) by the cross-linking reaction (see section IV-2, later), is independent of T_P's under the gelation conditions employed in this work.
(26) 3D image was constructed as follows. A total of 80 pieces of the sliced images, each of which consisted of 512×512 pixels^2, were taken at every 0.5 μm interval along the depth (or the incident beam) direction. The size of each pixel was 0.1563×0.1563 μm^2 and the focal depth and lateral resolution were estimated to be about 0.77 and 0.2 μm, respectively. The 80 sliced images were binarized with the same procedures as described in the previous paper.[27] The binarized sliced images were computationally stacked, and the interface was traced by the aid of computer to construct the 3D figure.
(27) Nishikawa, Y.; Jinnai, H.; Koga, T.; Hashimoto, T.; Hyde, T. *Langmuir* **1988**, *14*, 1242.
(28) Hyde, S.; Anderson, K.; Larsson, K.; Blum, Z.; Candh, T.; Lidin, S.; Ninham, B. W. *The Language of Shape*; Elsevier: Amsterdom, 1997.
(29) Hashimoto, T.; Jinnai, H.; Nishikawa, Y.; Koga, T. *Macromol. Symp.* **2002**, *190*, 9.
(30) Hashimoto, T. *Bull. Chem. Soc. Jpn.* **2005**, *78*, 1–39.
(31) It is important to note that the interface of this sponge-like structure in the gels is much rougher compared to the sponge-like phase-separated structure formed by the binary liquid mixtures. This is because the interface of the former is formed through the phase separation involving the elastic effects and that of the latter through the phase separation involving the hydrodynamic effects.[30]
(32) Jinnai, H.; Koga, T.; Nishikawa, Y.; Hashimoto, T.; Hyde, S. T. *Phys. Rev. Lett.* **1997**, *78*, 2248.
(33) Percus, J. K.; Yevick, G. *Phys. Rev.* **1985**, *110*, 1.
(34) Debye, P. *Physik. Z.* **1927**, *28*, 135.
(35) (a) Ornstein, L. S.; Zernicke, Z. *Proc. Akad. Sci. (Amsterdam)* **1914**, *17*, 183. (b) Ornstein, L. S.; Zernicke, Z. *Phys. Z.* **1918**, *19*, 134. (c) Ornstein, L. S.; Zernicke, Z. *Phys. Z.* **1926**, *217*, 761.
(36) It should also be noted that if the microgels are sufficiently small, $\Gamma_{shape}(r)$ is given by the delta function in eq 5, and $F(q)$ in eq 7 becomes constant, independent of q. Consequently, the scattering from thermal concentration fluctuations is given by the conventional Ornstein−Zernicke equation $[(1 + q^2\,\Xi^2)^{-1}]$.
(37) f_{micro}, f_{loose}, and f_{tight} are defined by $f_{micro} \equiv k_{micro}/k_t$, $f_{loose} \equiv k_{loose}/k_t$, and $f_{tight} \equiv k_{tight}/k_t$, respectively, with $k_t = k_{micro} + k_{loose} + k_{tight}$.
(38) It is noted that linear poly(NIPAAm) having weight average molecular weight $M_w = 3 \times 10^5$ (weight average DP, $N_w = 2.7 \times 10^3$) is synthesized, when the polymerization was performed under the same conditions as the gelation, except for the absence of a cross-linker. The radius of gyration of poly(NIPAAm), $R_{g,PNIAAm}$, is roughly 20 nm.[39] Although the estimated values ξ_{loose} are large, they are naturally still smaller than $R_{g,PNIPAAm}$.
(39) Kubota, K.; Fujishige, S.; Ando, I. *Polymer J.* **1990**, *22*, 15.
(40) The reaction rate of the NIPAAm and BIS as cross-linker is considered to be the same when the concentration ratio (NIPAAm/BIS = 133:1) and the facts that their chemical structure of NIPAAm are similar to that of BIS are taken into account.
(41) Hirokawa, Y.; Okamoto, T.; Kimishima, K.; Sakamoto, N.; Koga, T.; Yagi, N.; Okada, K.; Hashimoto, T. in preparation.
(42) The ϕ_P is estimated from the densities of NIPAAm (0.89) and water (1.00) without taking into account of volume change upon mixing.
(43) Even at $T_P = 24.5$ and 30.0 °C below the $T_{LCST} = 34$ °C for the linear poly(NIPAAm) solutions, it may be conceivable that the gelation process involves phase separation before the cross-linking reactions take place. This is because the rapid copolymerization of NIPAAm monomer and cross-linker into the copolymer chain generally generates the heat, which may transiently raise the temperature of the reacting system enclosed in the small cell above the T_{LCST}.[41] Moreover, it should be noted that the phase separation involved in the system here is the so-called "viscoelastic phase separation" inherent in the dynamically asymmetric systems.[30,44−49]
(44) Doi, M.; Onuki, A. *J. Phys. II* **1992**, *2*, 1631.
(45) Tanaka, H. *Macromolecules* **1992**, *25*, 6337.
(46) Onuki, A. *J. Non-Cryst. Solids* **1994**, *172*, 1151.
(47) Toyoda, N.; Takenaka, M.; Saito, S.; Hashimoto, T. *Polymer* **2001**, *42*, 9193.
(48) Onuki, A. *Phase Transition Dynamics*; Cambridge University Press: Cambridge, U.K., 2002.
(49) Takenaka, M.; Takeno, H.; Hasegawa, H.; Saito, S.; Hashimoto, T.; Nagao, M. *Phys. Rev. E.* **2002**, *65*, 021806.

MA800518T